Low-cost wavemeter with a solid Fizeau interferometer and fiber-optic input

Benedikt Faust and Lennart Klynning

A wavemeter suitable for measuring the wavelength of pulsed and continuous laser light has been constructed on the basis of a solid Fizeau interferometer (SFI). An accuracy of 1 part in 10^6 has been demonstrated in a range extending from 563 to 613 nm. The use of the SFI and of a combination of a single-mode optical fiber and an achromatic lens as a beam collimating system substantially simplifies the optical layout and reduces cost. The difficulties connected with the dispersion of the SFI have been overcome by an analytical description of the characteristics of the interferometer and accurate temperature stabilization.

Introduction

The application of tunable lasers in optical spectroscopy requires an absolute measurement of the wavelength of the produced radiation, since the adjustment parameters of the laser do not in most cases provide a sufficiently accurate estimate. Interferometric wavemeters, among which the Fizeau wavemeter is distinguished by the simplicity[1] of its design, have been shown to match the demands of ordinary spectroscopic applications. An additional benefit of the completely static Fizeau wavemeter is the possibility of using pulsed laser light. Generally, a Fizeau interferometer, which is formed by two slightly inclined planes, imposes a path difference of the two reflected rays (meeting at one point of the observation plane) that changes linearly across an arbitrary line of the observation plane, provided that the incident light is parallel. Thus an interference pattern with equally spaced fringes [given by Eq. (1)] is obtained along a line perpendicular to the apex line of the wedge formed by the two planes. By using, for example, a photodiode array this pattern can be converted to a computer-readable form and subsequently be processed to obtain the wavelength.

Previous investigations[2-4] and several commercial wavemeters have successfully used a vacuum-spaced Fizeau wedge. Therefore the required arrangement is, however, connected with a number of complications of the optical path due to dispersion in the front plate of the wedge and the required vacuum window.

A solid Fizeau wedge can substantially simplify the optics of the wavemeter. Investigations in this direction have already been carried out[5] and show that the difficulties have been shifted toward a more involved mathematical treatment because of dispersion inside the wedge. Moreover the strong temperature dependence of the refractive index of most materials requires accurate temperature stabilization of the wedge assembly.

In this work the properties of the interference pattern produced by a solid Fizeau interferometer (SFI) are described analytically, thus providing a model suitable for its interpretation. The construction of the wavemeter reported here follows the scheme in Fig. 1. Instead of the traditional pinhole as a spatial filter the end of an optical fiber has been favored, since it can couple the beam into the instrument without the need of realigning the optical components.

Theory of the SFI

The intensity of an interference pattern produced by the two-beam interference of plane monochromatic light reflected from two planes can, in its most general form, be described as

$$I(a) = I_0 \frac{1}{2}\left\{1 + \cos\left[2\pi a \frac{\partial p}{\partial a}\frac{1}{\lambda} + 2\pi \frac{p_{a=0}}{\lambda} + \pi\right]\right\}, \qquad (1)$$

where a is the coordinate along the line of observation, λ is the wavelength, $p_{(a=0)}$ is the optical path difference at the point where a is zero, $\partial p/\partial a$ is the partial derivative of the optical path difference with

The authors are with the Department of Physics, University of Stockholm, Vanadisvagen 9, 11346 Stockholm, Sweden.

Received 20 February 1991.
0003-6935/91/365254-06$05.00/0.

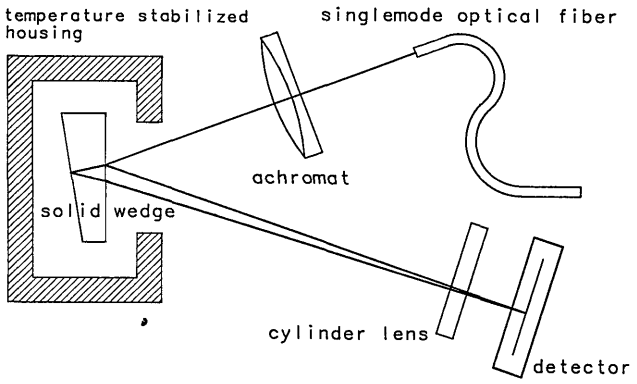

Fig. 1. Schematic view of the optical layout of a wavemeter using an SFI.

respect to this coordinate, and the additional π is a result of reflection at the front surface of the (optically thicker) wedge. The term $\lambda/(\partial p/\partial \alpha)$ represents the fringe spacing Λ:

$$\Lambda = \lambda \left(\frac{\partial p}{\partial \alpha}\right)^{-1}. \tag{2}$$

If we follow the procedure described in Ref. 6, the symmetry points of the observed cosine function can be determined, and the resulting loci curve can be fitted to obtain the fringe spacing Λ and the phase φ ($\varphi \in [-\pi, \ldots, +\pi]$) of the interference pattern from the slope and intercept of the fit. Because of the periodicity of the cosine, the measured phase φ reflects only the remainder that results from the division of $2\pi[p_{(\alpha=0)}/\lambda] + \pi$ by 2π. This drawback is, however, of no concern, if one can estimate the wavelength from Eq. (2) using Λ with an accuracy that is sufficient for determining the (integer) order o [see Eq. (16)] of interference, which allows, together with φ, a reconstruction of the complete phase. This phase can now deliver a better estimate for the wavelength.

The principal complication of the SFI is the fact that the quantities $\partial p/\partial \alpha$ and $p_{(\alpha=0)}$, which are constants for a vacuum-spaced wedge, are wavelength dependent for the SFI. It is thus desirable to find analytic functions expressing these quantities in terms of geometric parameters and the wavelength [by using a suitable model function $n(\lambda)$ for the index of refraction].

Therefore we assume (Fig. 2) that the detector line is placed under an angle ϑ to the front surface of the wedge. The thickness of the wedge at the foot of S_0 shall be e_0, and its angle shall be ϵ. The angle of incidence of the rays is α. A detailed consideration[7] shows that at any point (S, e) the sections $l_{12} = l_1 + l_2$, $l_{34} = l_3 - l_4$, m, and l_5 are given by the following equations (higher than quadratic orders in ϵ have been neglected):

$$l_{12} = e\frac{2n(1-\epsilon^2)}{g} + S\frac{2n\epsilon(\sin\alpha - 2g\epsilon)}{gh}, \tag{3}$$

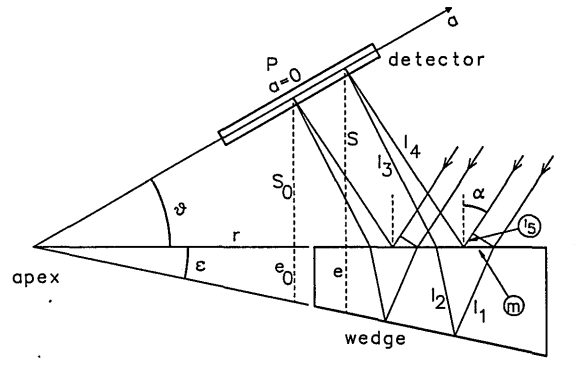

Fig. 2. Ray geometry in an SFI.

$$l_{34} = S\left(\frac{1}{h} - \frac{1}{\cos\alpha}\right), \tag{4}$$

$$m = 2e\frac{\epsilon g - \sin\alpha}{g} + S\frac{gh\tan\alpha - g(1-8\epsilon^2)\sin\alpha + 2\epsilon(g^2 - \sin^2\alpha)}{gh}, \tag{5}$$

$$l_5 = m\sin\alpha, \tag{6}$$

where the abbreviations $n = n_{SFI}/n_{air}$ for the effective index of refraction and

$$g = (n^2 - \sin^2\alpha)^{1/2}, \tag{7}$$

$$h = \{1 - [\sin\alpha(1-2\epsilon^2) - 2g\epsilon]^2\}^{1/2} \tag{8}$$

have been used. The term l_{12} represents the geometrical path difference that the penetrating ray experiences inside the wedge. Its first and most important term represents ignoring ϵ^2, the geometrical path difference in a planoparallel plate of the same thickness. The terms l_{34} and l_5 are geometrical path differences in the surrounding medium (presumably air), which shows that the SFI will have the small contribution of an air wedge. The term l_5 is due to a finite displacement m separating the reflection and refraction point. The optical path difference p can be calculated as follows:

$$p = n_{air}(nl_{12} + l_{34} + l_5). \tag{9}$$

Figure 3 shows p and its different contributions versus the angle of incidence calculated for an example geometry. With the constants S_0, e_0, ϵ, and α given, one thus obtains the quantity $p_{(\alpha=0)}$ required for the interpretation of the phase of the interference pattern.

To minimize the deviation from this model, which is introduced by a finite divergence or convergence of the incident beam, it is desirable to choose the line of observation so that

$$\frac{\partial}{\partial \sin\alpha} p = 0. \tag{10}$$

It can be shown that Eq. (10) is equivalent to $m = 0$

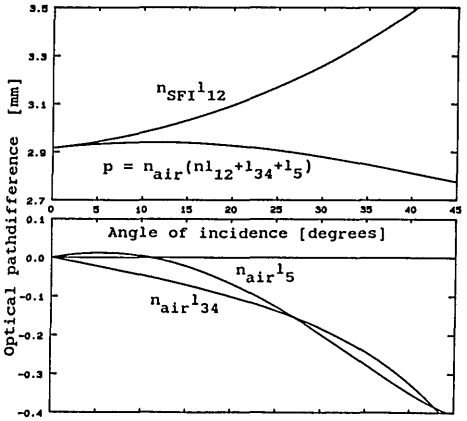

Fig. 3. Total path difference caused by the SFI and the path differences in the different sections, calculated for an SFI with e_0 = 1 mm, $\epsilon = 0.05°$, and S_0 = 100 mm at λ = 550 nm.

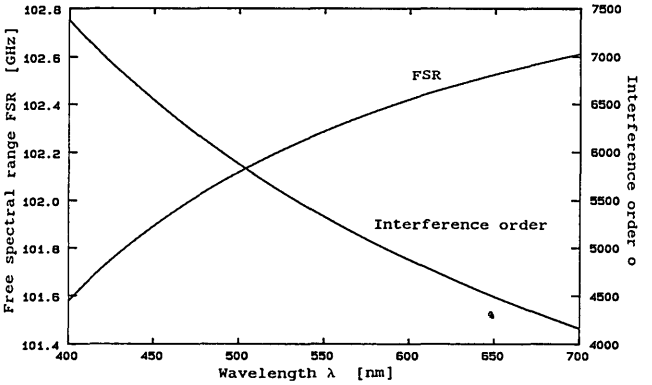

Fig. 4. Free spectral range and the interference order of the SFI, calculated for e_0 = 1 mm, $\alpha = 10°$, S_0 = 100 mm, and $\epsilon = 0.05°$.

(as seen qualitatively from Fig. 3), representing the zero-shear condition, which has the additional benefit of providing a maximum contrast of the interference pattern. By using Eq. (5) and neglecting quadratic orders in ϵ, we can thus obtain an expression relating S and e and defining the zero-shear line in which we have to place the detector:

$$S = e\frac{2h(\sin\alpha - g\epsilon)}{gh\tan\alpha - gs\sin\alpha + 2\epsilon(g^2 - \sin^2\alpha)}. \tag{11}$$

Substituting $e = r\tan\epsilon$ the angle ϑ_z of the detector with respect to the wedge, we obtain:

$$\tan\vartheta_z = \frac{S}{r} = \frac{2h\tan\epsilon(\sin\alpha_2 - g\epsilon)}{gh\tan\alpha - g\sin\alpha + 2\epsilon(g^2 - \sin^2\alpha)}. \tag{12}$$

Using ϑ_z the quantities S and e can be expressed in terms of the detector parameter a:

$$e = e_0 + a\cos\vartheta_z\tan\epsilon, \tag{13}$$

$$S = S_0 + a\sin\vartheta_z. \tag{14}$$

These expressions finally allow the calculation of the other parameter under question:

$$\begin{aligned}\frac{d}{da}p &= \frac{\partial e}{\partial a}\frac{\partial}{\partial e}p + \frac{\partial S}{\partial a}\frac{\partial}{\partial S}p,\\ &= \frac{2n_{air}n^2(1-\epsilon^2)}{g}\cos\vartheta_z\tan\epsilon\\ &+ \left[\frac{2n^2\epsilon(\sin\alpha - 2g\epsilon)}{gh} + \frac{1}{h} - \frac{1}{\cos\alpha}\right]n_{air}\sin\vartheta_z.\end{aligned} \tag{15}$$

In combination with Eq. (2) we obtain the fringe spacing. In contrast to a vacuum-spaced wedge the fringe spacing shows a slight deviation from linearity if plotted versus the wavelength.

Equation (9) will also deliver the order number and the free spectral range (FSR) of the interferometer by way of

$$o = \text{round}\left(\frac{p}{\lambda}\right), \qquad \text{FSR} = \frac{\partial\nu}{\partial m} = \frac{c}{p}. \tag{16}$$

These quantities are shown in Fig. 4 plotted versus the wavelength for an example geometry and the dispersion of quartz.[9]

Design Considerations

The essential part of the wavemeter is the SFI. From Fig. 3 and Eqs. (3) and (16), it is evident that the thickness e_0 of the SFI will be the most important parameter to influence the optical path difference and thus the order o of interference, which needs to be determined. Previous researchers[2] have shown that the usual level of spatial noise superimposed on an interference pattern with $\approx$50 fringes, sampled by 1024 photodiodes, limits the order number that can unambiguously be determined to the order of $\approx$10,000. This puts an upper limit of $\approx$3.5 mm (at n = 1.5) for e_0. Decreasing the order number (and at the same time e_0) will increase the precision of its estimation but simultaneously reduce the wavelength information contained in it. Moreover it poses considerable manufacturing problems[10] to produce an SFI thinner than 1 mm with the required surface quality. A thickness of 1 mm is thus a good compromise.

We can see from Eqs. (2) and (15) that the wedge angle ϵ is the main factor governing fringe spacing. Here we must satisfy two demands. We need a statistically significant number of fringes ($\approx$50) along the detector (Reticon RL1024G, 25 mm long) and a sufficient number of points in each fringe to determine the points of symmetry. An ϵ of $\approx 0.05°$ turns out to be a reasonable choice.

The material of the SFI is fused silica (Suprasil II, Heraeus), since its dispersion properties have been investigated thoroughly. The index of refraction can be modeled by Sellmeier's formula:

$$n^2 - 1 = \sum_{i=1}^{3}\frac{A_i\lambda^2}{\lambda^2 - a_i}. \tag{17}$$

The coefficients found in the literature[9] have been modified by a standard nonlinear least-squares fitting routine to obtain optimum matching of the values given by the manufacturer.

In the beam collimating system the end of a single-mode optical fiber (core diameter, 10 μm), which approximates a point source and thus reduces the spatial noise, and an achromatic doublet (Melles-Griot $f_{\text{eff}} = 400$ mm, $d = 40$ mm), which produces a parallel beam, have been employed. The lens, compared to a parabolic mirror, was chosen to reduce cost. It has, however, the disadvantage that the still present chromatic aberration causes a small divergence of the beam.

By applying Newton's lens formula it can be shown that a long focal length can minimize this effect. The focal length is, however, limited by the desirable dimensions of the instrument. In the wavelength range of 450–700 nm, the distance of a virtual point source can be kept to > 200 m. The errors caused by the finite divergence of the beam are smaller than the one produced by the inhomogeneous illumination[6] of the interferometer. Because of dispersion inside the SFI, the zero-shear position that is given by Eq. (11) will suffer a shift of the order of 1 mm for the parameter set used here and in a wavelength interval extending from 450 to 700 nm. The shift in path difference caused hereby can be calculated and added as a correction in Eq. (9).

As shown above, a displacement m close to zero is desirable. The finite beam divergence, however, makes it necessary also for the derivative $\partial m/\partial \sin\alpha$ to reach the minimum as well in order to achieve this. From Fig. 3 it can be seen that this situation occurs for α close to 5° and moreover that the path difference $n_{\text{air}} l_{34}$ decreases with decreasing α, which reduces the, however small, errors introduced by changes in air pressure. Reducing the angle α of incidence is severely limited by the zero-shear distance S_0 approaching zero simultaneously. This leads in practice to the problem that the detector partly shadows the beam incident on the SFI. An α larger than 10° is therefore given by practical considerations. (The shadowing can be avoided by use of a beam splitter for illumination[4] or decreased by using off-axis geometry[11] where the detector is rotated by 90°.)

The introduction of a short focal length cylindrical lens in front of the detector has proved to enhance considerably the sensitivity of the wavemeter. The quality of the observed interference pattern was, however, largely damaged by the insufficient surface quality of our lens. Therefore the use of the lens has been suspended.

The mechanical stability of the optical components against thermal and seismic influences is essential, since the accuracy of the wavemeter depends on the fringe position on the detector. This applies in particular to the position of the detector with respect to the SFI. A lateral shift in the pattern as small as 1 μm will result in a wavelength error of about 1 in 10^6. For this reason the detector has been kept in position by quartz rods 10 mm in diameter, which offer a low expanson coefficient.

An additional complication of the design is the need for temperature stabilization of the SFI. It is primarily the index of refraction that is affected by temperature changes. The thermal shift of the refractive index of quartz amounts according to Ref. 9 to approximately $+12 \times 10^{-6}\ \text{K}^{-1}$. Thus one can estimate the change Δo of the interference order resulting from the 1 K temperature change, when one considers only the biggest contribution to the path difference, which is given by the first term of Eq. (3):

$$\frac{\partial p}{\partial n} \approx \frac{2 n_{\text{air}} n e_0}{g}\left(2 - 2\frac{n}{g}\right) \approx 2.63\ \text{mm} \rightarrow \Delta p$$

$$\approx 1\ \text{K} \times 2.63\ \text{mm} \times 12 \times 10^{-6}\ \text{K}^{-1} \approx 31.4 \times 10^{-6}\ \text{mm}$$

$$\lambda = 0.55\ \mu\text{m} \rightarrow \Delta o \approx 0.057. \quad (18)$$

To obtain an accuracy of $\pm 1{:}10^7$ at an order number of $o = 5000$, it is necessary to stabilize the temperature to better than ±0.009 K.

To achieve this the SFI was placed in an oven that allows the beam to travel in and out through a thin slit (Fig. 5). The SFI is mounted close to a heat sink supplied by a resistor heating element. The usual materials that improve heat conduction, e.g., silicon grease, cannot be employed, since they change the reflection properties of the back plane and thus worsen the fringe contrast. For this reason, a small

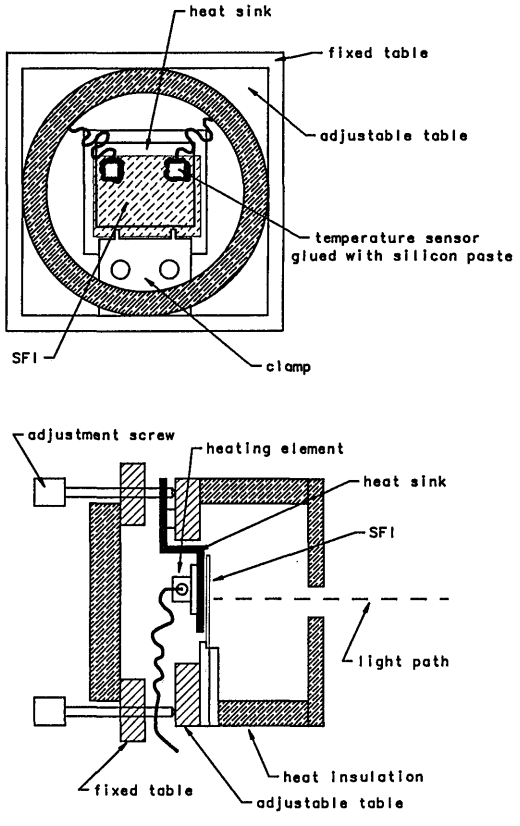

Fig. 5. Isometric view of the arrangement containing the SFI sectioned through the center.

air gap (0.1 mm) is maintained between the SFI and the heat sink. To avoid reflections the heat sink is covered with soot. Two temperature sensors are glued onto the front surface of the SFI using silicon grease. One of them is used for temperature stabilization and the second one to monitor the temperature. With the arrangement shown and a pulse-width-modulated servo amplifier a stability of ±0.02 K/100 h could be achieved.

Calibration and Evaluation

The photodiode array was embedded in a dedicated hardware,[7] which interfaced it to a 68000 microcomputer connected by a serial link to a terminal. An algorithm for successive digital filtering of the interference pattern[6] was employed to determine the fringe spacing and the phase of the pattern in the reference point. To calculate the wavelength based on these data, the parameters α, ϵ, ϑ, S_0, and e_0 must be known.

The α term can be measured from the apparatus with sufficient accuracy. The ϑ and S_0 terms were calculated by using Eq. (12), approximate values for the other constants, and a mean value for n and were subsequently adjusted in the apparatus.

The fringe spacing and phase were then measured at around ten different wavelengths between 563 and 613 nm provided by an Autoscan CR-699-29 ring laser system combined with an iodine cell[12] as a reference standard with an accuracy of $\approx \pm 150$ MHz. With the spacing values a nonlinear least-squares fitting of Eq. (2) was carried out to determine ϵ. Concerning e_0 a heuristic search within a reasonable expectation interval was carried out. It minimized the residuals resulting from Eq. (9). Thus the most consistent e_0 could unambiguously be found.

For wavelength calculations based on fringe spacing and phase, an inversion of the functions $\Lambda(\lambda)$ and $\varphi(\lambda)$ is convenient. This inversion, however, poses substantial difficulties, as can be seen from Eqs. (2), (15), (9), and (17). It is thus done indirectly by iteration until $\Lambda(\lambda)$, $\varphi(\lambda)$ match the measured values.

System Performance

The absolute accuracy and the reproducibility of the measurements are the qualities that interest us most. The above-mentioned laser system has been used to produce 19 different wavelengths that have been measured by the wavemeter. The results are shown in Table I. A maximum deviation of 0.00073 nm equaling 1.3 parts in 10^6 and an rms value of 0.00044 nm equaling 0.8 parts in 10^6 of accuracy were observed. Besides the random scattering of the errors, which is partly caused by the insufficient accuracy of the method with which the laser system has been brought to the center of the individual iodine lines, a systematic decrease in the errors can be seen. A probable explanation is that the model function for the refractive index does not provide sufficient accuracy (because of erroneous values that have been used in the fitting).

In Fig. 6 the fluctuations in the φ phase and the SFI temperature during a period of 2 h and 28 min are shown. At the end the wavelength has been changed leading to a phase jump. Even though the two quantities are measured at different locations (10 mm) on the SFI, a slight correlation can be observed, corresponding to the index change in order of magnitude and sign. It can be concluded that, since the precision and reproducibility of the phase measurements are better than ±1/1000 of a free spectral range, the wavelength measurements achieve a precision of better than ±100 MHz, which equals 2 parts in 10^7. Because of systematic errors, however, this cannot be exploited in terms of absolute accuracy.

Table I. Results of Wavelength Measurements

Spacing (Diodes)	Phase $\vartheta' = \vartheta/\pi$ (−0.5, . . . , 0.5)	λ_1 (nm)	m	λ_2 (nm)	λ (nm)	Residuals λ_2 (nm)
8.6417978	−0.0656019	563.5928739	5089	563.6184948	563.617878	+0.000617
8.6880981	0.0380713	566.5673748	5062	566.5685450	566.568150	+0.000387
8.7412127	0.1315421	569.9798610	5031	569.9976229	569.997045	+0.000578
8.7804598	−0.0613629	572.5015407	5009	572.4861803	572.486353	−0.000173
8.8194608	−0.2241598	575.0075191	4987	574.9935932	574.993726	−0.000132
8.8579085	−0.0428299	577.4780625	4965	577.4840629	577.484040	+0.000024
8.8966998	−0.2220739	579.9707869	4943	579.9226884	579.922935	−0.000247
8.9363748	−0.3226681	582.5204104	4921	582.4898994	582.490058	−0.000159
9.0128660	0.2341530	587.4362587	4880	587.4856761	587.485614	+0.000062
9.0507123	−0.2306423	589.8686584	4859	589.9258355	589.925173	+0.000663
9.0922083	0.3780760	592.5357397	4837	592.4986476	592.499366	−0.000719
9.1295022	0.1951619	594.9328355	4817	594.9471791	594.947286	−0.000107
9.1690782	−0.4762881	597.4767032	4797	597.4764424	597.476595	−0.000152
9.2068795	−0.3207734	599.9065891	4777	599.9252158	599.924823	+0.000387
9.2487838	0.3125432	602.6003112	4755	602.5847826	602.585085	−0.000302
9.2858262	0.4141883	604.9815892	4736	604.9572001	604.957666	−0.000466
9.3269470	−0.4161721	607.6251337	4715	607.5942833	607.595012	−0.000729
9.3647638	−0.3929719	610.0563534	4696	610.0171621	610.017527	−0.000365
9.4021080	0.4751975	612.4572712	4678	612.4798223	612.479994	−0.000171

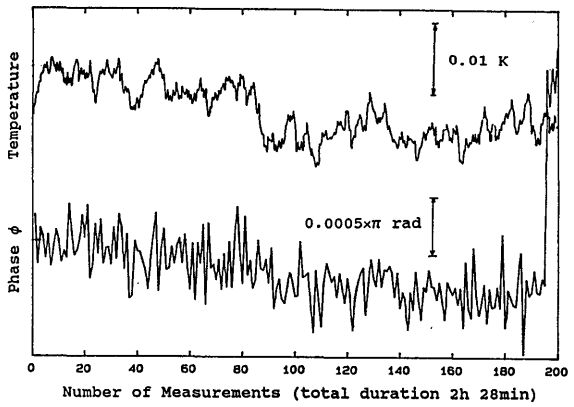

Fig. 6. Phase φ of the interference pattern and the temperature of the SFI recorded simultaneously for 2 h and 28 min at λ = 578.873 nm.

Conclusion

A Fizeau wavemeter with an SFI that gives an absolute accuracy of 1 part in 10^6 in the wavelength interval of Rhodamine 6G has been constructed and successfully tested. The characteristics of the interference pattern produced by the SFI have been analytically described, leading to a better understanding of its specific properties. Alignment problems and the cost of the system could be considerably reduced by use of an optical fiber in combination with an achromatic lens as a beam collimating system.

The occurrence of systematic errors, which are most likely caused by an erroneous refractive index, leads to the conclusion that the wavelength range can be extended considerably if more accurate values of n are available.

The authors thank D. Kürbitz, Carl Zeiss Co., Oberkochen, Germany, for providing a carefully manufactured SFI.

References

1. J. J. Snyder, "Laser wavelength meters," Laser Focus **18**(5), 55–61 (1982).
2. M. B. Morris, T. J. McIllrath, and J. J. Snyder, "Fizeau wavemeter for pulsed laser wavelength measurement," Appl. Opt. **23,** 3862–3868 (1984).
3. D. F. Gray, K. A. Smith, and F. B. Dunning, "Simple compact Fizeau wavemeter," Appl. Opt. **25,** 1339–1343 (1986).
4. J. L. Gardner, "Compact Fizeau wavemeter," Appl. Opt. **24,** 3570–3573 (1985).
5. C. Reiser and R. B. Lopert, "Laser wavemeter with solid Fizeau wedge interferometer," Appl. Opt. **27,** 3656–3660 (1988).
6. J. J. Snyder, "Algorithm for fast digital analysis of interference fringes," Appl. Opt. **19,** 1223–1225 (1980).
7. B. Faust, "Aufbau eines Wellenlangenmessgerates mit massiver Fizeau-Keilplatte," diploma thesis Institut für Angewandte Physik, Universität Bonn, Bonn, Germany, 1990).
8. M. Born and C. Wolf, *Principles of Optics* (Pergamon, London, 1959), p. 290 *ff.*
9. I. H. Malitson, "Interspecimen comparison of the refractive index of fused silica," J. Opt. Soc. Am. **55,** 1205 (1965).
10. D. Kürbitz, Fa. Carl Zeiss, Oberkochen, Germany (personal communication, 1990).
11. J. L. Gardner, "Wavefront curvature compensation in a Fizeau wavemeter," Appl. Opt. **25,** 3799–3800 (1986).
12. S. Gerstenkorn and P. Luc, *Atlas du Spectre d'Absorption de la Molecule d'Iode, Complement* (Editions du CNRS, Paris, undated).